Materials Characterization 133 (2017) 60–69

Contents lists available at ScienceDirect

Materials Characterization

journal homepage: www.elsevier.com/locate/matchar

Three-dimensional characteristics of the grain boundary networks of conventional and grain boundary engineered 316L stainless steel

Tingguang Liu[a,c], Shuang Xia[a,b,*], Bangxin Zhou[a,b], Qin Bai[a], Gregory S. Rohrer[d]

[a] Institute of Materials, School of Materials Science and Engineering, Shanghai University, Shanghai 200072, China
[b] State Key Laboratory of Advanced Special Steel, Shanghai University, Shanghai 200072, China
[c] National Center for Materials Service Safety, University of Science and Technology Beijing, Beijing 100083, China
[d] Department of Materials Science and Engineering, Carnegie Mellon University, Pittsburgh, PA 15213, USA

ARTICLE INFO

Keywords:
316L stainless steel
3D EBSD
Grain boundary engineering
Quadruple junction
Grain-cluster

ABSTRACT

The three-dimensional microstructures of two conventional 316L stainless steel and a grain boundary (GB) engineered one of the same material have been characterized by serial sectioning and electron backscatter diffraction (EBSD) mapping. The twin boundaries arrangement in the grain boundary network were investigated and compared. Although the triple junction character distribution and quadruple junction character distribution were improved slightly by grain boundary engineering, considerably higher proportions of triple junctions with two twin boundaries and quadruple junctions with three twin boundaries were formed after GB engineering, which will be more beneficial to the resistance to intergranular degradation. Large grain-clusters formed in the GB engineered material, and the topology structures of them are complex tree-ring shape twin-chain. In comparison, the grain-clusters in conventional material are small, having simple tree shape twin-chain.

1. Introduction

Grain boundary (GB) engineering [1–9] has been proposed to control and design the grain boundary network of polycrystalline materials as the phenomenon had been found that some so-called special boundaries have better performance than random boundaries, such as lower boundary energy and stronger resistance to impurities segregation/precipitation [10] and intergranular degradation [9,11–15]. The GB related properties of materials can be improved by GB engineering due to the GB network optimization. A quantitative parameter that evaluates the degree of optimization of the GB network is the proportion of special boundaries [4,5,12–22]. Generally, the proportion can be increased to more than 75% from about 40%, which has been realized in austenitic stainless steel [12,13], Ni based alloy [14,18,19] and Cu based alloy [3]. Actually, about 80% of these special boundaries are twin boundary [18,19], so the twin boundary plays the most important role in GB engineering.

Besides the proportion of twin boundaries, the arrangement of twin boundaries in the GB network should be taken into account when we study the GB engineered microstructures, such as the connectivity of twin boundaries or random boundaries [4,12,13,16,23]. The improvement of properties of materials, such as intergranular corrosion and intergranular stress corrosion cracking [11–15], are substantially resulted from disrupting the random boundary connectivity [12,16,24,25]. The percolation theory [26] is widespread applied to quantify the connectivity of boundaries with certain characters. However, the connectivity strongly depends on the observation dimensions for the same system [26,27]. As an example, the connectivity of random boundaries could be broken when the proportion of special boundaries is more than 0.35 in 2D microstructure [28–30], but the threshold proportion is approximately 0.8 for 3D microstructure [26].

In addition, the connectivity of random boundaries depends on not only the proportion of special boundaries but also the arrangement of special boundaries in the GB network. If boundaries with different characters distribute randomly in 3D space, the threshold proportion of special boundaries to disrupt the random boundary connectivity is 0.775, but it is about 0.80–0.85 if the distribution is constrained by texture or crystallography rule [26], such as the combination rule of $\Sigma 3^n$ boundaries at triple junction and quadruple junction [31–35], where the Σ-value indicates the boundary character according to coincidence site lattice (CSL) model [23,36]. The Σ-value of twin boundary is 3. The maximum number of twin (Σ3) boundaries in a triple junction is two, then the third boundary is Σ9 [35]. Six boundaries meet at a quadruple junction, but the misorientations of only three of them are independent [35]. The maximum number of Σ3 boundaries in a quadruple junction is three, and then the other three boundaries

* Corresponding author at: (S. Xia) P.O. Box 269, 149 Yanchang Road, Shanghai 200072, China.
E-mail addresses: xs@shu.edu.cn, xiashuang14@sohu.com (S. Xia).

http://dx.doi.org/10.1016/j.matchar.2017.09.026
Received 11 December 2016; Received in revised form 20 September 2017; Accepted 21 September 2017
Available online 22 September 2017
1044-5803/ © 2017 Elsevier Inc. All rights reserved.

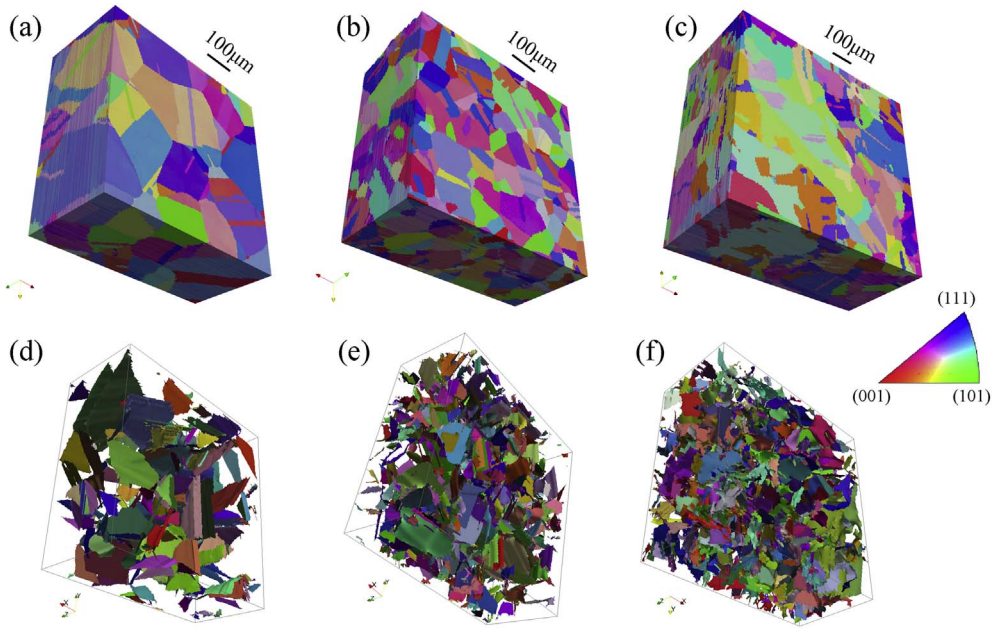

Fig. 1. Visualizations of the three 3D-EBSD microstructures and spatial distributions of twin boundaries in the three samples: 316LL (a, d), 316LS (b, e) and 316LGBE (c, f). They have dimensions 600 μm × 600 μm × 267.6 μm, 600 μm × 600 μm × 257.5 μm and 800 μm × 800 μm × 377.3 μm, respectively. The color is consistent with the inverse pole figure (IPF) color code of direction Z. (For interpretation of the references to color in this figure legend, the reader is referred to the web version of this article.)

are constrained, with two Σ9 and one Σ27 [35]. Triple junction can be observed in 2D maps, but the arrangement of twin boundaries in quadruple junction must be visualized in 3D space.

The arrangement of boundaries with different Σ-values is consistent with the mechanism of GB network evolution during GB engineering [6,8,17–20,34,37]. Multiple twinning has been believed the reason to form the high proportion of $\Sigma 3^n$ boundaries. During recrystallization, the face-centered-cubic materials of low and medium stacking fault energy are prone to twinning operations [38–44]. An iterative process of twinning operations starting from a single nucleus occurs in the wake of the recrystallization fronts migrating, which is named multiple twinning [6,34,37,45–49]. The assembly of all twins formed by the multiple twinning starting from a single nucleus is named grain-cluster or twin-related domain [6,8,17–20,34,37]: all inner boundaries are of $\Sigma 3^n$ misorientations, and the outer boundaries are crystallographically random, and all inner grains form a twin-chain [20,45,48,50]. Large grain-cluster is a prominent characteristic of the GB engineered microstructure [3,19,20,51].

This paper compares the grain boundary network of a GB engineered 316L stainless steel with that of conventional materials in 3D, studying the effects of GB engineering on GB network, such as the arrangement of twin boundaries in triple junction and quadruple junction, grain-cluster and twin-chain.

2. Experiments

2.1. Materials

The three 316L stainless steel specimens used in this work are designated as 316LL, 316LS and 316LGBE and were produced from the same starting material. The starting 316L material is a conventional, commercially available stainless steel product. The 316LL and 316LS samples were produced by hot rolling followed by full recrystallization. Both were rolled to a 50% reduction in thickness at 1000 °C. The 316LL (316LS) sample was recrystallized with a 2.5 h (0.5 h) anneal at 1050 °C (1000 °C). The grain size of 316LL is greater than that of 316LS.

The grain boundary engineered stainless steel (316LGBE) was produced from the same commercially available 316L. The as-received specimen was hot-rolled to a 50% reduction of thickness (using a starting temperature of 1000 °C) and then water quenched. It was then annealed at 1000 °C for 30 min and water quenched. Next, it was warm rolled to a 5% reduction of thickness (using a starting temperature of 400 °C) and then water quenched. In the final step, it was annealed at 1100 °C for 1 h and then water quenched. After this treatment, it was about 19 mm thick. The GB engineering procedure of "warm-rolling with low-strain deformation combined with high temperature annealing" was carried out to create a high fractional population of twin boundaries, as described previously [17–19]. With this procedure, it is possible to produce grain boundary engineered specimens with large dimensions.

2.2. 3D Data Acquisition

Serial-sectioning coupled with EBSD mapping [36] was used to obtain the 3D microstructure data [52–55]. First, the samples were mechanically-polished by hand under a fixed load and for fixed times. A suspension of sol-gel produced alumina (0.05 μm) was used for the polishing. Second, a micrometer and precision thickness gauge were used to measure the reduction in thickness, with a precision of 1 μm. Third, micro-hardness indents were used to mark the region of interest for EBSD collection. Finally, the orientations of the crystals on the polished surface were measured by 2D EBSD mapping. The EBSD (HKL/Channel 5) system was integrated with a CamScan Apollo 300 field emission scanning electron microscope (SEM). The EBSD field of view was 600 μm × 600 μm with a step size of 2.5 μm for specimen 316LL and 316LS. For 316LGBE, the field of view was 800 μm × 800 μm and the step size 5 μm. The orientations in 101 parallel sections were mapped for 316LL and 316LS. For 316LGBE, 70 parallel sections were mapped. The average thicknesses per section were 2.65 μm, 2.55 μm and 5.39 μm for specimen 316LL, 316LS and 316LGBE, respectively.

2.3. Post-processing of 3D EBSD Data

The 3D reconstruction of the EBSD data was carried out in Dream.3D v4.2.5004 [56], and ParaView v4.3.1 [57] was used for the visualization. Dream.3D [21,56,58,59] was used to quantify grain sizes, grain orientations, and the number of nearest neighbors, and to identify the twin boundaries based on Brandon criterion [60]. In addition, the number of twin boundaries per grain, the number of twin boundaries neighboring a boundary, the number of twin boundaries per triple junction and per quadruple junction, and the reconstruction of grain-clusters were performed by using DREAM.3D coupled with in house

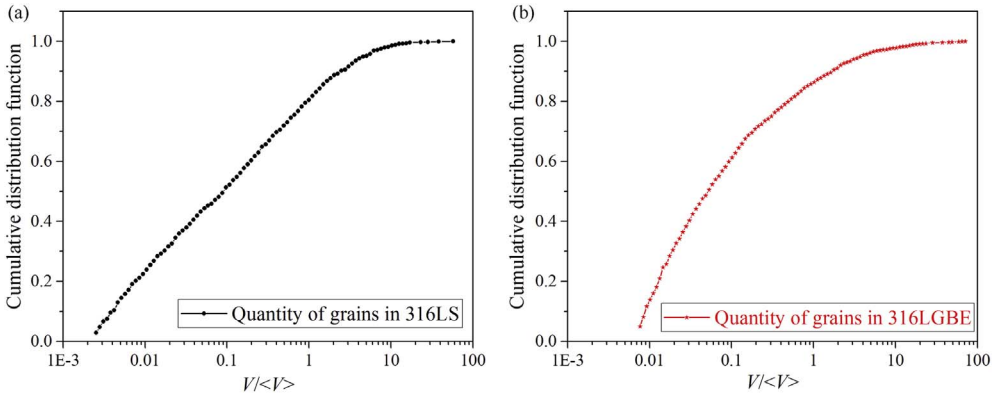

Fig. 2. Cumulative distributions of grain volumes (V) in 3D microstructures of the conventional sample 316LS (a) and the GB engineered sample 316LGBE (b), where $\langle V \rangle$ means average grain volume. It is 56,520 μm^3 for 316LS, and 158,458 μm^3 for 316LGBE.

developed Matlab programs.

3. Results

Visualizations of the three microstructures are illustrated in Fig. 1. Specimen 316LL, 316LS and 316LGBE contain 440 grains, 1540 grains and 1543 grains (including the grains that intersect the borders of specimen volume), respectively. The three samples had average grain volumes of 215,290 μm^3 (equivalent sphere diameter 74.9 μm), 56,520 μm^3 (48.8 μm), and 158,458 μm^3 (38.3 μm), respectively. Fig. 2 shows the grain size distributions of the conventional stainless steel 316LS and the GB engineered one 316LGBE. In both samples, many grains have much smaller sizes than the average size, but some large grains that several decuples of the average exist as well. Fig. 1(d, e, f) show the spatial distributions of all twin boundaries in the three sample, respectively. It seems that all the three samples have uniform distributions of twin boundaries. The area fractions of twin boundaries in the 3D-EBSD microstructures are 39.8% (316LL), 42.9% (316LS) and

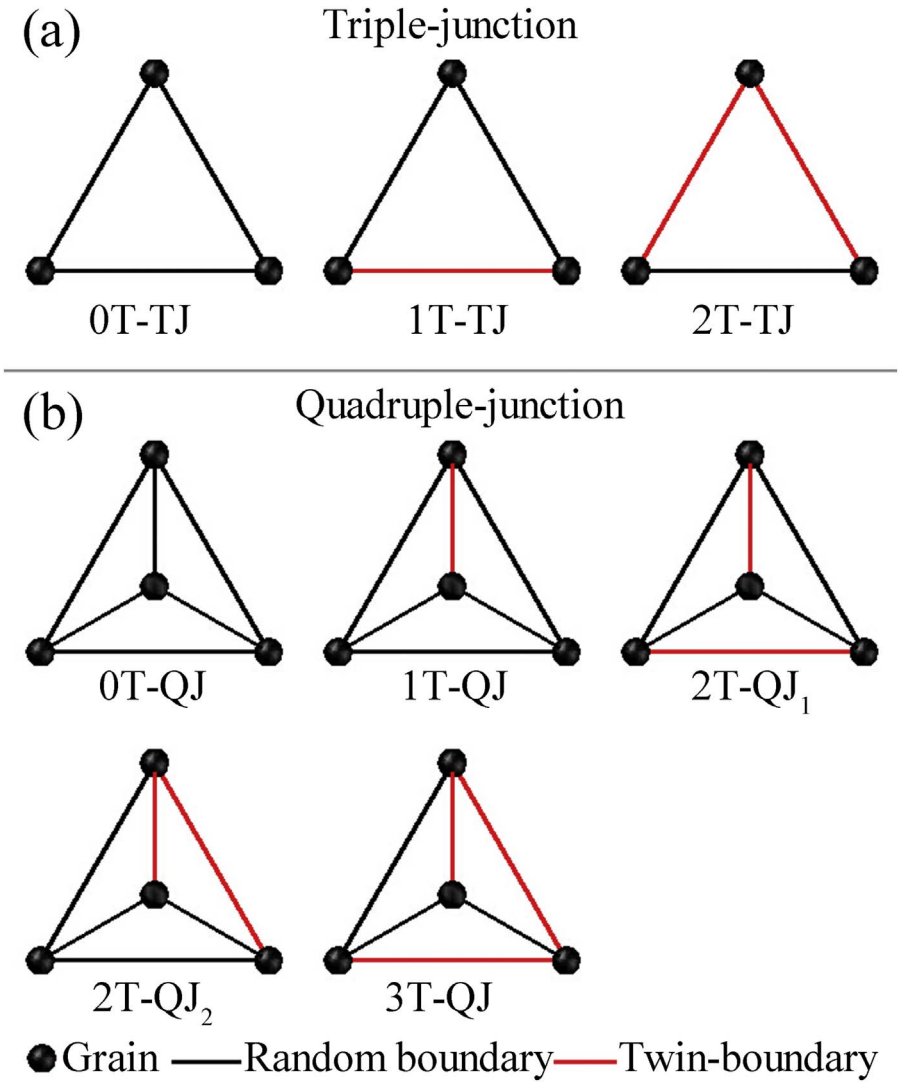

Fig. 3. Topology structures of triple junctions (a) and quadruple junctions (b) with different numbers of twin boundaries, where points represent grains and lines represent grain boundaries. The twin boundaries are colored red. (For interpretation of the references to color in this figure legend, the reader is referred to the web version of this article.)

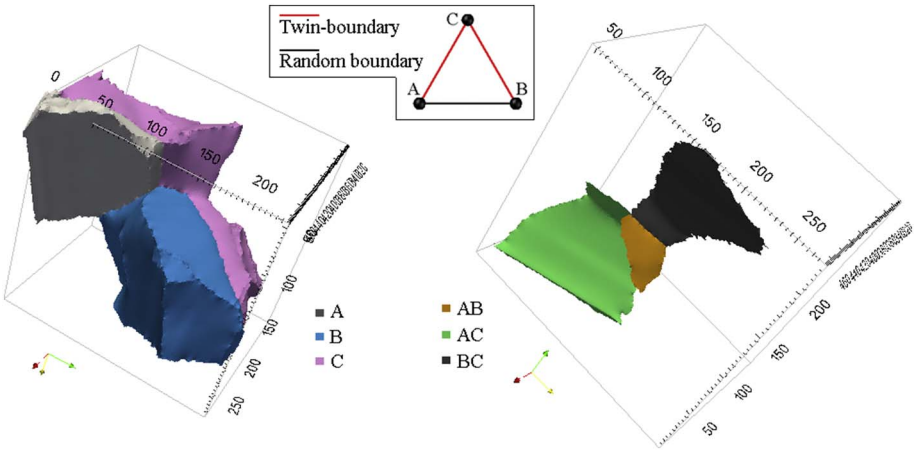

Fig. 4. An example of triple junction with two twin boundaries (2T-TJ) from sample 316LL and its topology structure: the assembly of the three mutually neighboring grains and the three boundaries between them.

58.7% (316LGBE), respectively, and their twin boundary quantity fractions are 18.1%, 18.0% and 19.8%. In addition, the quantities of twin boundaries in substructures of grain boundary network and grain-clusters will be investigated in the following sections.

3.1. Twin Boundaries in Triple Junction

Three boundaries meet at a triple junction (TJ) [26,61–64], where has a common line (triple-line) [64]. In other words, three grains meet at a triple junction. A classification method of triple junctions is topologically shown in Fig. 3(a) according to the number of twin boundaries: 0T-TJ, 1T-TJ and 2T-TJ, where points represent grains, and red line indicates twin boundaries, and black lines indicate random boundaries or low-Σ CSL boundaries except Σ3. 0T-TJ, 1T-TJ and 2T-TJ mean triple junctions that have zero, one and two twin boundaries, respectively. A triple junction has two twin boundaries at most [35]. Fig. 4 illustrates an example of 2T-TJ from sample 316LL, where another boundary should be Σ9 according to CSL theory [35]. It should be mentioned here that Dream3D [56], the 3D EBSD processing software, could not identify other low-Σ CSL boundaries except Σ3.

Distributions of triple junction character for the three samples 316LL, 316LS and 316LGBE are shown in Fig. 5. The average numbers of twin boundaries per triple junction are 0.53, 0.61 and 0.73 for the three samples, respectively. It is highest for the GB engineered sample. The GB engineered sample has higher proportions of 1T-TJ and 2T-TJ than the conventional samples, but the proportions of triple junctions

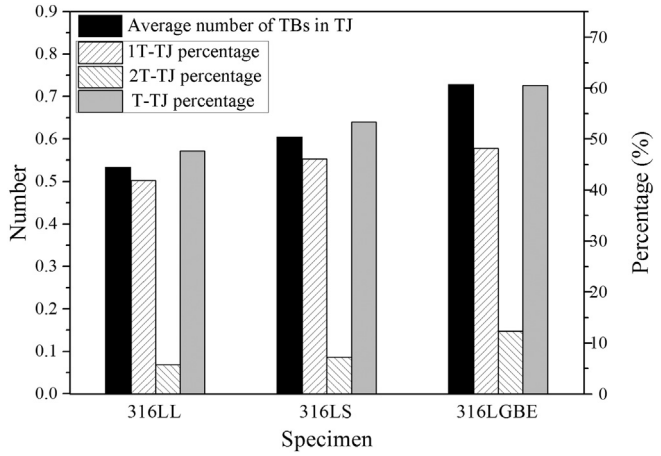

Fig. 5. Distributions of triple junction (TJ) character for the three samples 316LL, 316LS and 316LGBE: the average numbers of twin boundaries per triple junction, and the proportions of triple junctions with one (1T-TJ) and two (2T-TJ) twin boundaries and the summation proportions (T-TJ), respectively.

with two twin boundaries are quite low for all samples. The proportions of 2T-TJ are only 5.8%, 7.2% and 12.3% for the three samples, respectively. In total, about 60% of triple junctions have one twin boundary at least in the GB engineered sample, which is higher than that in the conventional samples.

3.2. Twin Boundaries in Quadruple Junction

Four mutually neighboring grains meet at a quadruple junction (QJ), where has six boundaries and a common point (quadruple-node) [64–67]. Gertsman [35] studied the combination rule of $\Sigma 3^n$ boundaries at quadruple junction, inferring that the maximum number of twin boundaries in a quadruple junction is three, with two Σ9 boundaries and one Σ27 boundary in this case. As an example shown in Fig. 6, the quadruple junction has three twin boundaries. The other type of low-Σ CSL boundaries cannot be identified by Dream3D, but the orientations of the four grains are known, as shown in Table 1, and thus all the misorientations of the six boundaries can be calculated, which are illustrated in Table 1 as well. It can be confirmed that the quadruple junction has three twin boundaries, two Σ9 boundaries and one Σ27 boundary.

According to the number and arrangement of twin boundaries, quadruple junctions are classified into five types: 0T-QJ (quadruple junction with one twin boundary), 1T-QJ, 2T-QJ_1, 2T-QJ_2 and 3T-QJ, as topologically shown in Fig. 3b. Isomerism structure was taken into account, such as 2T-QJ_1 and 2T-QJ_2. Both have two twin boundaries but different topology structures.

The quadruple junction character distribution had been considered in this study, but the current software (Dream3D coupled with in-house developed Matlab programs) cannot quantify quadruple junction. Instead of quadruple junction, a new concept of quadruple union was proposed here, which is the assembly of four mutually neighboring grains, among which there are six boundaries but they are not necessarily meeting at a point. If they meet at a point, the quadruple union is a quadruple junction. Quadruple union obeys the same combination rule of $\Sigma 3^n$ boundaries with the quadruple junction, and has the same topology structure and classification as shown in Fig. 3b. In 3D microstructures, quadruple unions can be identified and quantified by using Dream3D and our in-house developed Matlab programs.

The quadruple union character distributions for the three samples are shown in Fig. 7. The average numbers of twin boundaries per quadruple union are 1.08, 1.12 and 1.40 for sample 316LL, 316LS and 316LGBE, respectively. Quadruple union in the GB engineered sample has more twin boundaries than that in the conventional samples on average. The proportion of quadruple unions with more twin boundaries is lower for all samples. Compared with conventional samples, the proportion of 1T-QU (quadruple union with one twin boundary) is lower in the GB engineered sample, but the proportions of 2T-QU and

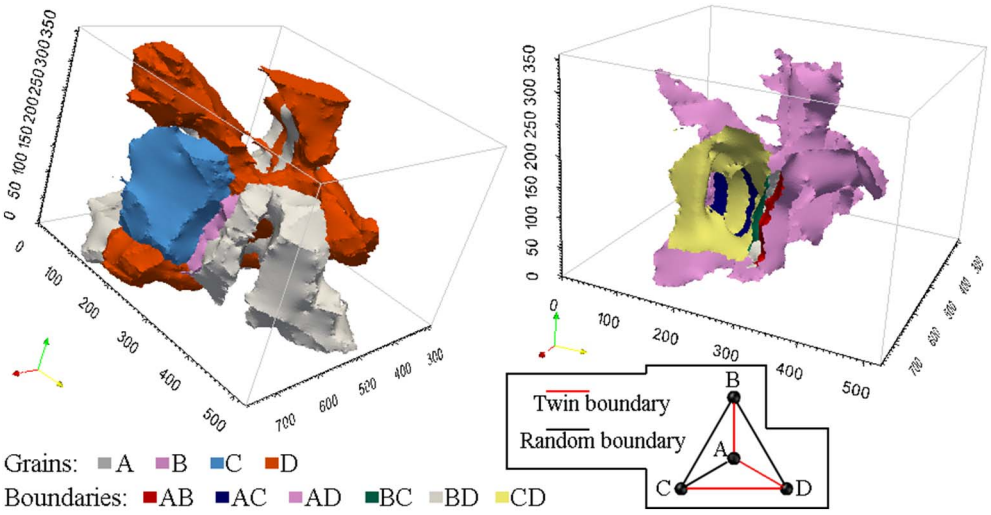

Fig. 6. An example of quadruple junction with three twin boundaries (3T-QJ) in sample 316LGBE and its topology structure: the assembly of the four mutually neighboring grains and the six boundaries among them.

3T-QU are obviously higher, which are more beneficial to stop a crack than 1T-QU as discussed below. In total, about 85% of quadruple unions has at least one twin boundary in the GB engineered sample, which is slightly higher than that in the conventional samples.

3.3. Twin Boundaries per Grain

It is common to approximate grains as polygons with a fixed number of faces or boundaries. The samples 316LL, 316LS and 316LGBE have 9.6, 11.2 and 9.5 boundaries per grain on average, respectively. The boundaries of a grain have different misorientations or Σ-values. It has been found that the twin boundaries have stronger resistant to intergranular degradation than random boundaries [11–15], so more twin boundaries of a grain contribute to prevent the grain dropping from the matrix during intergranular corrosion. The average numbers of twin boundaries per grain are 1.71, 2.00 and 1.81 for the three samples, respectively. Compared with conventional samples, grains in the GB engineered sample do not have more twin boundaries on average. This result is consistent with the low proportion of twin boundaries in number after GB engineering, though the proportion in area is very high.

Fig. 8(a & b) show the correlation of the number of twin boundaries per grain with the number of boundaries per grain in specimen 316LS and 316LGBE, respectively. The grain with more boundaries is prone to having more twin boundaries regardless of GB engineering, and the correlations are fit linear functions. The slope of the fitting line is larger for the GB engineered sample than that for the conventional sample, which means that the ratio of twin boundary quantity to boundary quantity per grain on average should be higher for the GB engineered sample, although its average number of twin boundaries per grain is

Table 1
Orientations of the four grains in the quadruple junction of Fig. 6, and misorientations of the six boundaries among them.

Grain ID		Orientation: Euler angles, °		
A	g344	251.4	45.5	129.4
B	g659	337.3	18.8	14
C	g411	286.3	29.1	38.5
D	g778	55.7	25.3	327.5
Boundary		θ, [hkl]		CSL
Misorientation	AB	59.6, [1 −1 1]		Σ3
	AC	37.8, [0 −1 −1]		Σ9
	AD	58.8, [−1 −1 −1]		Σ3
	BC	31.7, [1 0 −1]		Σ27a
	BD	39.2, [1 0 −1]		Σ9
	CD	59.5, [−1 −1 1]		Σ3

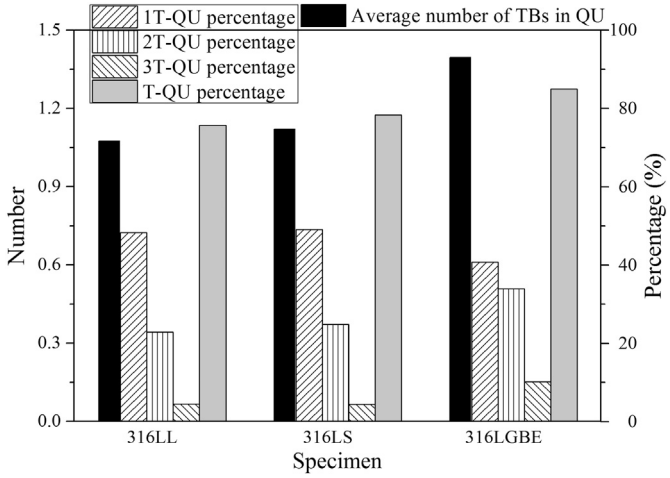

Fig. 7. Distributions of quadruple union (QU) character for the three samples 316LL, 316LS and 316LGBE: the average numbers of twin boundaries per quadruple union, and the proportions of quadruple unions with one (1T-QU), two (2T-QU) and three (3T-QU) twin boundaries and the summation proportions (T-QU), respectively.

lower. The 20.3% of the boundaries per grain are twin boundaries in the GB engineered sample 316LGBE, and the ratio is 17.0% for the conventional sample 316LS, but it should be pointed out that the distribution for sample 316LS (Fig. 8a) is comparatively dispersed. Some grains have large residual that is the deviation of observed value and the fitting line.

The dropping-resistance of a grain during intergranular corrosion is correlated with not only the boundaries of the grain but also the neighboring boundaries of the grain. Neighboring boundaries of a grain include all boundaries of the grain and all boundaries that have a common line or point with the grain. The average numbers of neighboring boundaries per grain are 33.3, 40.6 and 33.7 for sample 316LL, 316LS and 316LGBE, and the average numbers of neighboring twin boundaries per grain are 5.97, 8.00 and 7.71 for the three samples, respectively. The grains in GB engineered sample do not have more neighboring twin boundaries compared with the grains in conventional samples. However, the ratio, number of neighboring twin boundaries to number of neighboring boundaries per grain, is a little larger for the GB engineered sample, as shown in Fig. 8(c & d). 22.2% of the neighboring boundaries per grain are twin boundaries in the GB engineered sample, and the ratio is 19.7% for the conventional sample.

In a similar way, the cracking susceptibility of a boundary is correlated not only with the character of the boundary itself but also the

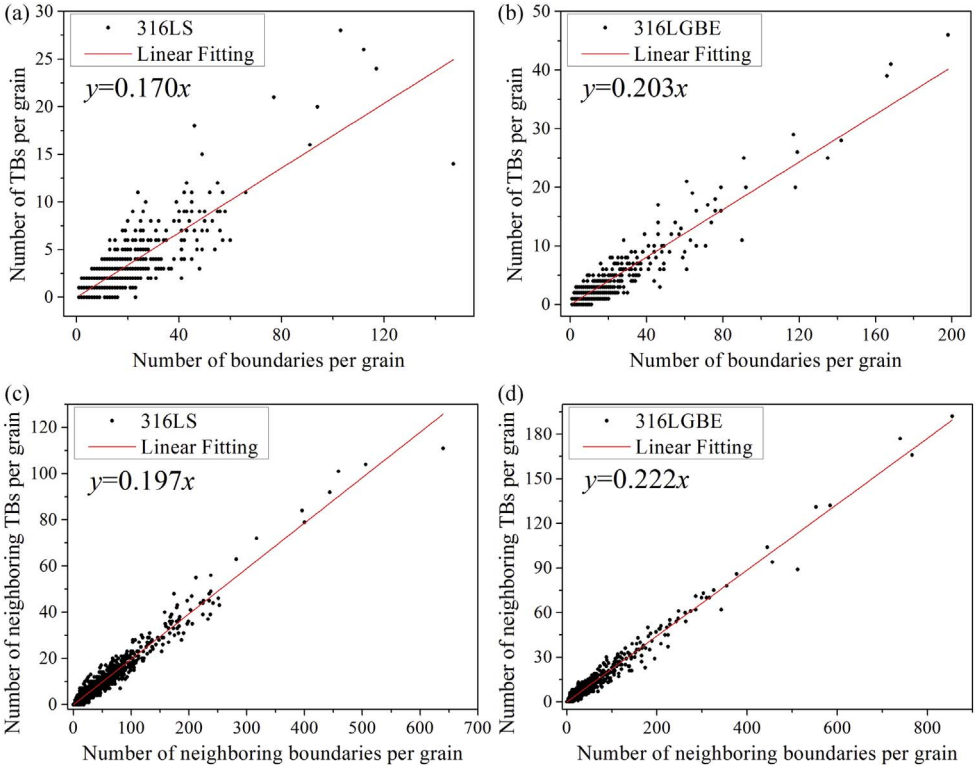

Fig. 8. (a, b) Plots of the number of twin boundaries with the number of boundaries per grain in sample 316LS and 316LGBE, and their linear fits. (c, d) Plots of the number of neighboring twin boundaries with the number of neighboring boundaries per grain in the two samples, and their linear fits. The neighboring boundaries of a grain include all boundaries of the grain and all boundaries that have common line or point with the grain.

characters of its neighboring boundaries. The neighboring boundaries of a boundary include all boundaries that have a common line with the boundary. As an example, if a cracking susceptive boundary (random boundary) is surrounded by cracking resistant boundaries (twin boundaries), it would never crack during intergranular corrosion, because the crack has no way to access to the boundary. The average numbers of neighboring boundaries per boundary are 9.2, 9.5 and 8.8 for the three samples, respectively, in which 1.72, 1.97 and 2.22 are twin boundaries on average. The boundaries in GB engineered sample have more neighboring twin boundaries on average than that in conventional sample. Fig. 9 shows the correlation of the neighboring twin boundary quantity with the neighboring boundary quantity per boundary in specimen 316LS and 316LGBE. The fitting line slope is obviously higher for the GB engineered sample than that for the conventional sample. In addition, in Fig. 9, the random boundaries and twin boundaries are illustrated separately. Compared with twin boundaries, the random boundaries are prone to having more neighboring twin boundaries in both conventional and GB engineered sample.

In addition, compared with the conventional sample 316LS, the GB engineered sample 316LGBE has larger average grain size, but the average number of (neighboring) boundaries per grain for 316LGBE is smaller than that of 316LS because the average boundary size is larger for 316LGBE. On the other hand, the largest number of (neighboring) boundaries per grain for 316LGBE is larger than that of 316LS, as shown in Fig. 8. This is associated with the grain size distribution. Fig. 2 shows that 316LGBE has some extremely large grains which are about 70 times larger than the average volume, and 316LS has some the largest grain which is 57 times larger than its average volume. The largest grain of 316LGBE is much larger than that of 316LS, so the largest grain of 316LGBE has more (neighboring) boundaries as well as twin boundaries.

3.4. Grain-cluster

Large grain-cluster is a prominent characteristic of the GB engineered microstructure besides the high proportion of twin-related boundaries [13,15,18–20]. The grain-cluster is formed by multiple twinning starting from a single nucleus [6,34,37,45–49], so a grain-cluster can be determined by counting twins, twins of twins and so on starting from a grain. This was performed using an in-house developed Matlab program. Fig. 10 shows the statistics of grain-clusters in sample

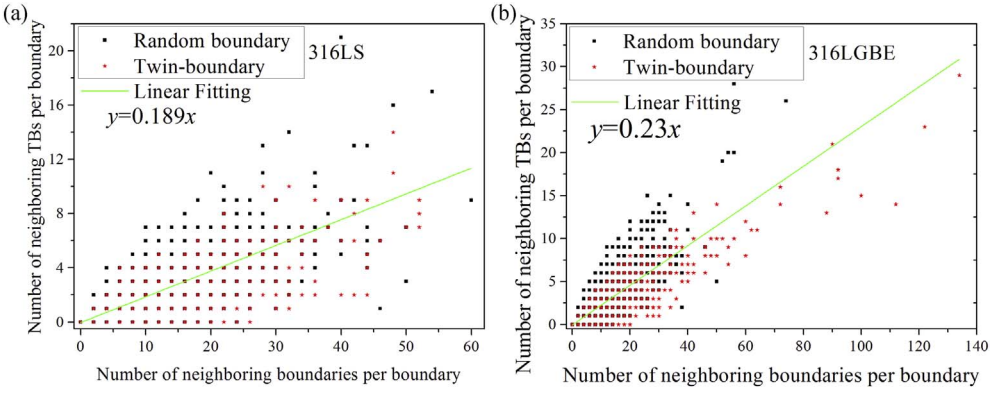

Fig. 9. Plots of the number of neighboring twin boundaries with the number of neighboring boundaries per boundary in sample 316LS (a) and 316LGBE (b), and their linear fits, and the random boundaries and twin boundaries are shown by black points and red stars, respectively. The neighboring boundaries of a boundary include all boundaries that have common line with the boundary. (For interpretation of the references to color in this figure legend, the reader is referred to the web version of this article.)

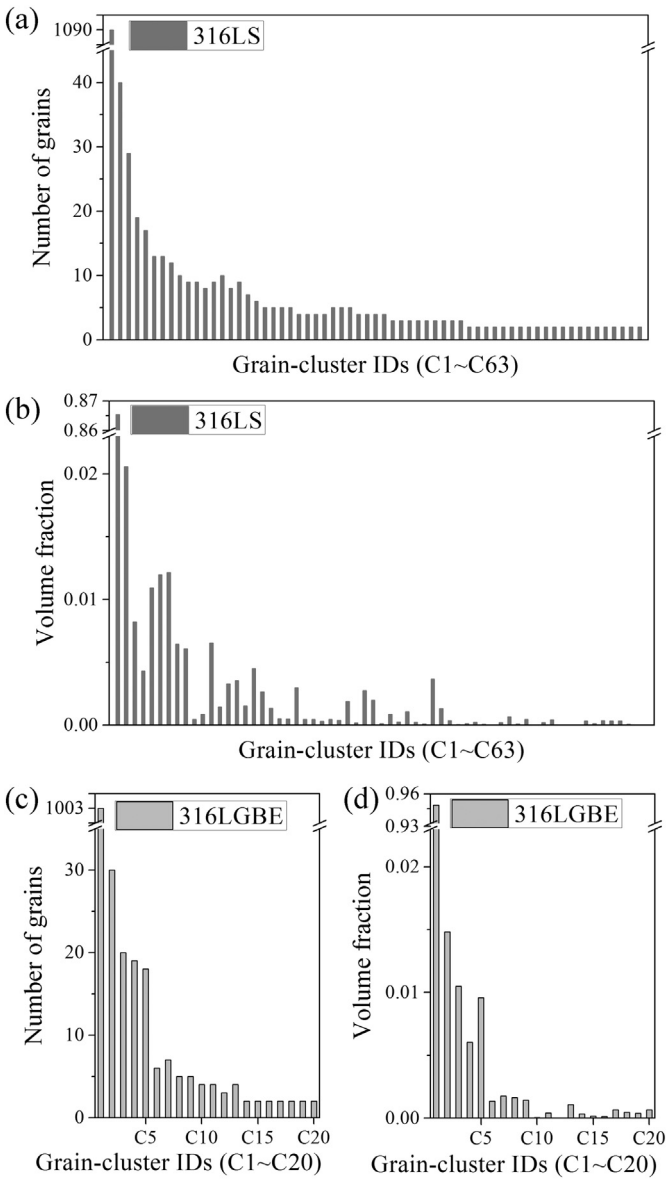

Fig. 10. Statistics of grain-clusters in sample 316LS (a, b) and 316LGBE (c, d). They have 63 and 20 grain-clusters, respectively.

316LS (Fig. 10a & b) and 316LGBE (Fig. 10c & d). The number of grains and the volume fraction for each grain-cluster were calculated. The conventional sample has 63 grain-clusters, and the GB engineered sample has 20 grain-clusters. Both samples have several grains without twins, which are not included in Fig. 10.

2D studies show that GB engineered materials have much larger grain-clusters than conventional materials [18,19]. Kumar et al. [8] quantified and compared the grain-clusters in GB engineered and conventional coppers in 3D, finding similar results with the 2D studies. However, Fig. 10 shows that the grain-cluster distributions are similarly for the samples before and after GB engineering, and surprisingly both samples have an extremely large grain-cluster, which takes up most of the total grains and the volume of each sample. The largest grain-clusters in the two sample have 1090 and 1003 grains, and the total number of grains is 1540 (316LS) and 1543 (316LGBE) for the two sample, respectively. These abnormal results are correlated with the post-processing of the 3D data.

A grain-cluster is formed by multiple twinning starting from a single nucleus [6,34,37,45–49], so grain-clusters should be identified according to their formation history. However, it is impossible to determine grain-clusters by tracing the formation history. In this work, the grain-clusters were determined by twin boundaries. All grains that can be chained by twin boundaries were determined as one grain-cluster. However, the twin boundaries can be classified into three types according to the formation mechanisms: (i) twin boundaries formed by twinning operations [38–44]; (ii) twin boundaries that formed by encounter of twins that formed by a multiple twinning process starting from a single nucleus (these grains naturally have $\Sigma 3^n$-misorientation, so encounter of these grains may form twin boundaries.); (iii) twin boundaries formed by random encounter of grain growth (except the case of ii) [44]. According to the formation mechanism of grain-cluster, the assembly of grains that can be chained by type-i & ii twin boundaries is a grain-cluster. However, we cannot separate the type-iii twin boundaries from type-i & ii, so neighboring grain-clusters that formed by different multiple twinning processes starting from different nuclei may be determined as one grain-cluster due to the type-iii twin boundaries.

4. Discussion

4.1. Grain Boundary Network

2D studies [13–15,68] has shown that the triple junctions with two twin boundaries (2T-TJ) could stop the crack propagation. This is a primary reason that GB engineered microstructure has stronger resistance to intergranular degradation. High proportion of 2T-TJ is a greatly desired result of GB engineering [14,16]. The present 3D study shows that the proportion of 2T-TJ increased obviously after GB engineering (from about 7% to 12.3%), but, disappointingly, it is still too low. This is consistent with the low proportion of twin boundaries in number (19.8%), although the proportion in area is quite high (58.7%) after GB engineering because some large twin boundaries formed in the GB engineered sample. (An in-depth discussion on this topic was carried out in another under review paper titled “Three-dimensional study of grain boundary engineering effects on the grain boundary character distribution of 316L stainless steel”.) Therefore, higher proportion of twin boundaries in number is more important to improve properties of materials. Advanced procedures of GB engineering that could produce high proportion of twin boundaries not only in length/area but also in number should be developed.

While the 2T-TJ has been believed a necessary structure to stop crack propagation according to 2D studies [13–15,68], the triple junction cannot represent characteristics of 3D GB network. Quadruple junction is the smallest structure element retaining 3D characteristics of GB network [35]. The maximum number of twin boundaries in a quadruple junction is three, as shown in Fig. 3. In this case, the four grains of the quadruple junction will be bound together by the three twin boundaries, even if all the other three boundaries damaged by a crack. Therefore, in 3D, quadruple junctions with three twin boundaries (3T-QJ) will stop the crack propagation.

4.2. Topology Structure of Grain-cluster

The twin boundaries in the GB engineered microstructure are not randomly distributed but forming grain-clusters due to the formation mechanism of multiple twinning [6,34,37,45–49]. 2D studies had demonstrated that the GB engineered materials have much larger grain-clusters than conventional materials [18,19]. However, in the present 3D study, the grain-cluster statistics illustrate similar distributions between the conventional and GB engineered samples, as shown in Fig. 10. The reason is that the statistics did not reveal their substantial differences, which will be discussed by using the topology structure of grain-clusters.

Fig. 11 shows the twin-chain of grain-cluster C2 and C3 in sample 316LS and 316LGBE, respectively. They are the second and the third largest grain-clusters in related sample. The numbers of grains in C2

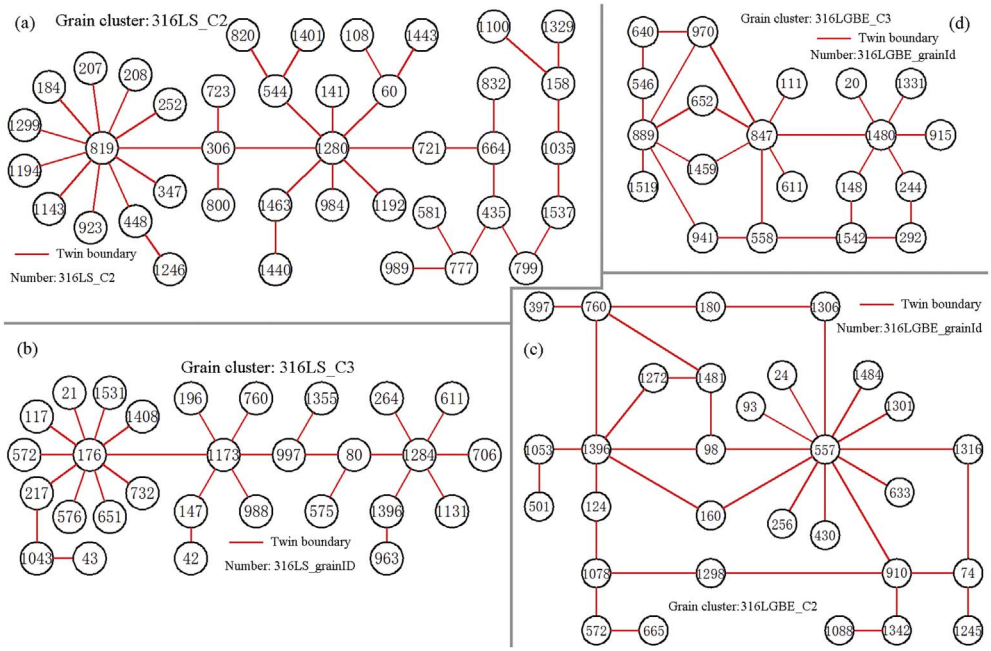

Fig. 11. Twin-chains of grain-clusters 316LS-C2/C3 (a, b) and 316LGBE-C2/C3 (c, d). They are the second and the third largest grain-cluster in the two samples, respectively. The circles represent grains in which the numbers are grain ID, and red lines represent twin boundaries. (For interpretation of the references to color in this figure legend, the reader is referred to the web version of this article.)

and C3 are 30 (40) and 20 (29) for 316LGBE (316LS). The twin-chains of C2 and C3 of the conventional sample are simple tree-shape, as shown in Fig. 11(a & b). Comparatively, the topology structures of C2 and C3 in the GB engineered sample are complex tree-ring-shape, as shown in Fig. 11(c & d).

Next, we want to check whether the determined grain-cluster by Dream3D is formed by a multiple twinning process starting from a single nucleus or is a combination of different grain-clusters. Fig. 12a shows the recalculated twin-chain of the grain-cluster 316LGBE-C2 according to the grain orientations, in which the misorientations of boundaries along the longest chain are illustrated in the figure. The twin boundary formed by twinning operation (type-i) should have small deviation from the standard twin relationship (60° [1 1 1]), but type-iii twin boundary should have large deviation generally. In Fig. 12a, all twin boundaries have small deviation, so they should be type-i or ii twin boundaries formed by a multiple twinning, except that four Σ81d boundaries (60.4° [−4 3 4] [23]) were determined as Σ3 by Dream3D, as shown by the cyan lines in Fig. 12a. The grain-cluster 316LGBE-C2 should form by a multiple twinning starting from a single nucleus except for grains 572 and 665.

Fig. 12d shows the longest chain of the grain-cluster 316LS-C2 (Fig. 11a), and the misorientations of boundaries in the chain were recalculated. Most of these misorientations have small deviation from the standard twin relationship, but there are three boundaries have large deviation. They are g306/g1280, g721/g664 and g779/g1537. The three twin boundaries should be type-iii, so the twin-chain illustrated in Fig. 11a is not formed by one multiple twinning. The observed large grain-cluster C2 (determined by Dream3D) in the conventional sample 316LS is actually a combination of several small grain-clusters that formed by different multiple twinning processes starting from different nuclei. Similarly, the extremely large grain-cluster C1 of 316LS should consist of many small grain-clusters. In comparison, the extremely large grain-cluster C1 of 316LGBE should consist of many grain-clusters, but these grain-clusters are relatively larger than that in 316LS, and they have complex tree-ring-shape twin-chains like Fig. 12a.

On the other hand, if a twin-chain was formed by a multiple twinning process starting from a single nucleus, there should have a type-ii

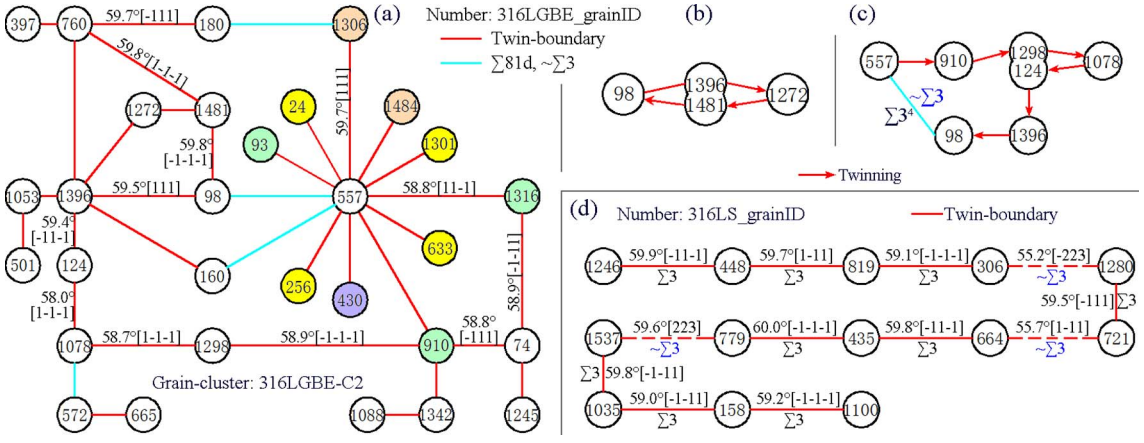

Fig. 12. (a) Recalculated twin-chain of the grain-cluster 316LGBE-C2, in which the twins of grain g557 were colored according to their orientations. The misorientations of boundaries along the longest chain were recalculated according to the grain orientations. (b) A ring substructure in the twin-chain of grain-cluster 316LGBE-C2, and a possible twinning route to form the ring chain illustrated by arrows. The grain g1396 and g1481 have the same orientation. (c) Another ring substructure in the twin-chain of grain-cluster 316LGBE-C2, and a possible twinning route to form the chain. (d) The longest chain in the grain-cluster 316LS-C2 (Fig. 11a) and recalculated misorientations. (For interpretation of the references to color in this figure legend, the reader is referred to the web version of this article.)

Table 2
Orientations of the grains in Fig. 12(c), and the calculated misorientations and nearest CSL values of boundaries between these grains.

Grain	Euler angles, °			Boundary	Misorientation	CSL value
g557	121.2	51.5	224.0			
g910	196.7	15.9	118.4	g557/g910	58.8°, [−1 1 −1]	Σ3
g1298	85.0	42.2	277.7	g910/g1298	58.9°, [−1 −1 −1]	Σ3
g1078	164.9	39.2	175.5	g1298/g1078	58.7°, [1 −1 −1]	Σ3
g124	83.7	40.6	281.0	g1078/g124	58.0°, [1 −1 −1]	Σ3
g1396	350.9	25.2	325.7	g124/g1396	59.4°, [−1 1 −1]	Σ3
g98	54.3	56.4	326.9	g1396/g98	59.5°, [1 1 1]	Σ3
g557	121.2	51.5	224.0	g98/g557	60.3°, [−2 3 −3]	Σ81d

twin boundary in a ring-substructure of the twin-chain. As an example, Fig. 12b shows a ring-substructure in the twin-chain 316LGBE-C2. The misorientation of the boundary g98/g1396 is 59.5° [1 1 1], and all the other three boundaries have misorientation of 59.8° [1 1 1]. So a possible twinning-route to form the ring-substructure is g1396 → g1272 → g1481 → g98 by twinning operations. The grain g98 and g1396 encountered due to grain growth and formed a type-ii twin boundary. The two grains g1396 and g1481 have the same orientation. Another possible twinning-route to form the ring-substructure is g1396 → g1272 → g1481 → g98 → gX, where the hypothetical grain gX has the same orientation with g1396, and they encountered during grain growing. In this case, all twin boundaries in the ring-substructure are type-i.

In addition, a ring-substructure of twin-chain should have even number of grains according to the multiple twinning process, but ring-substructure with odd number of grains were observed in Fig. 11(c & d). For example, Fig. 12(c) shows a ring-substructure of the grain-cluster 316LGBE-C2. The misorientations of boundaries in this ring-substructure were recalculated, as shown in Table 2, finding that the boundary g98/g557 is Σ81d actually, but it was determined as Σ3 by Dream3D. Other boundaries have small deviation from the standard twin-relationship, so a possible twinning-route to form the ring-substructure chain is shown by arrows in Fig. 12c. Grain g1298 and g124 have the same orientation, so the *n*-value of the $\Sigma 3^n$-misorientation between grain g557 and g98 is 4, although 6 independent twinning operations occurred between them.

5. Conclusions

This paper quantitatively compared the grain boundary network of a 316L stainless steel after GB engineering with that of conventionally processed materials. The area proportion of twin boundaries of the GB engineered sample was much higher than that of the conventional samples, but they have similar proportions of twin boundaries in quantity. The distributions of triple junction character, quadruple junction character and number of twin boundaries per grain shown that the GB network was optimized slightly by GB engineering. However, the proportions of triple junction with two twin boundaries and quadruple junction with three boundaries had considerably increase after GB engineering (from about 7% to 12.3% and from about 4.5% to 10.2%), which are more beneficial to stop a crack. Another significant difference between the GB engineered and conventional microstructures is the grain-cluster. The grain-clusters in GB engineered material are larger, and their topology structures are more complex compared with that of the conventional materials.

Acknowledgements

This work was supported by the National Natural Science Foundation of China (NSFC) (grant number 51671122) and Shanghai Science and Technology Commission (grant number 13520500500). The authors gratefully thank X.T. Zhong (Carnegie Mellon University) for her help in Dream3D and ParaView.

References

[1] T. Watanabe, Approach to grain boundary design for strong and ductile polycrystals, Res. Mech. 11 (1984) 47–84.
[2] G. Palumbo, K.T. Aust, Structure-dependence of intergranular corrosion in high purity nickel, Acta Metall. Mater. 38 (1990) 2343–2352.
[3] V. Randle, Mechanism of twinning-induced grain boundary engineering in low stacking-fault energy materials, Acta Mater. 47 (1999) 4187–4196.
[4] M. Kumar, A.J. Schwartz, W.E. King, Microstructural evolution during grain boundary engineering of low to medium stacking fault energy fcc materials, Acta Mater. 50 (2002) 2599–2612.
[5] V. Randle, M. Coleman, A study of low-strain and medium-strain grain boundary engineering, Acta Mater. 57 (2009) 3410–3421.
[6] T.G. Liu, S. Xia, H. Li, B.X. Zhou, Q. Bai, The highly twinned grain boundary network formation during grain boundary engineering, Mater. Lett. 133 (2014) 97–100.
[7] S. Kobayashi, R. Kobayashi, T. Watanabe, Control of grain boundary connectivity based on fractal analysis for improvement of intergranular corrosion resistance in SUS316L austenitic stainless steel, Acta Mater. 102 (2016) 397–405.
[8] J. Lind, S.F. Li, M. Kumar, Twin related domains in 3D microstructures of conventionally processed and grain boundary engineered materials, Acta Mater. 114 (2016) 43–53.
[9] E.M. Lehockey, G. Palumbo, On the creep behaviour of grain boundary engineered nickel, Mater. Sci. Eng. A 237 (1997) 168–172.
[10] H. Li, S. Xia, B. Zhou, W. Chen, C. Hu, The dependence of carbide morphology on grain boundary character in the highly twinned Alloy 690, J. Nucl. Mater. 399 (2010) 108–113.
[11] P. Lin, G. Palumbo, U. Erb, K.T. Aust, Influence of grain boundary character distribution on sensitization and intergranular corrosion of alloy 600, Scr. Met. Mater. 33 (1995) 1387–1392.
[12] M. Michiuchi, H. Kokawa, Z.J. Wang, Y.S. Sato, K. Sakai, Twin-induced grain boundary engineering for 316 austenitic stainless steel, Acta Mater. 54 (2006) 5179–5184.
[13] C.L. Hu, S. Xi, H. Li, T.G. Liu, B.X. Zhou, W.J. Chen, N. Wang, Improving the intergranular corrosion resistance of 304 stainless steel by grain boundary network control, Corros. Sci. 53 (2011) 1880–1886.
[14] K. D, S. Mandal, C.N. A., D.-I. Kim, B. de Boer, S.S. V., Implication of grain boundary engineering on high temperature hot corrosion of alloy 617, Corros. Sci. 106 (2016) 293–297.
[15] S. Xia, H. Li, T.G. Liu, B.X. Zhou, Appling grain boundary engineering to Alloy 690 tube for enhancing intergranular corrosion resistance, J. Nucl. Mater. 416 (2011) 303–310.
[16] M. Kumar, W.E. King, A.J. Schwartz, Modifications to the microstructural topology in f.c.c. materials through thermomechanical processing, Acta Mater. 48 (2000) 2081–2091.
[17] S.A. Xia, B.X. Zhou, W.J. Chen, Effect of single-step strain and annealing on grain boundary character distribution and intergranular corrosion in Alloy 690, J. Mater. Sci. 43 (2008) 2990–3000.
[18] T.G. Liu, S. Xia, H. Li, B.X. Zhou, Q. Bai, C. Su, Z.G. Cai, Effect of initial grain sizes on the grain boundary network during grain boundary engineering in Alloy 690, J. Mater. Res. 28 (2013) 1165–1176.
[19] T.G. Liu, S. Xia, H. Li, B.X. Zhou, Q. Bai, Effect of the pre-existing carbides on the grain boundary network during grain boundary engineering in a nickel based alloy, Mater. Charact. 91 (2014) 89–100.
[20] S. Xia, B.X. Zhou, W.J. Chen, Grain cluster microstructure and grain boundary character distribution in Alloy 690, Metall. Mater. Trans. A 40a (2009) 3016–3030.
[21] M. Groeber, S. Ghosh, M.D. Uchic, D.M. Dimiduk, A framework for automated analysis and simulation of 3D polycrystalline microstructures. Part 1: statistical characterization, Acta Mater. 56 (2008) 1257–1273.
[22] K. Kurihara, H. Kokawa, S. Sato, Y.S. Sato, H.T. Fujii, M. Kawai, Grain boundary engineering of titanium-stabilized 321 austenitic stainless steel, J. Mater. Sci. 46 (2011) 4270–4275.
[23] V. Randle, The Role of the Coincidence Site Lattice in Grain Boundary Engineering, Cambridge University Press, London, 1996.
[24] E.M. Lehockey, A.M. Brennenstuhl, I. Thompson, On the relationship between grain boundary connectivity, coincident site lattice boundaries, and intergranular stress corrosion cracking, Corros. Sci. 46 (2004) 2383–2404.
[25] G. Palumbo, P.J. King, K.T. Aust, U. Erb, P.C. Lichtenberger, Grain boundary design and control for intergranular stress-corrosion resistance, Scr. Met. Mater. 25 (1991) 1775–1780.
[26] M. Frary, C.A. Schuh, Connectivity and percolation behaviour of grain boundary networks in three dimensions, Philos. Mag. 85 (2005) 1123–1143.
[27] E.A. Holm, P.M. Duxbury, Three-dimensional materials science, Scr. Mater. 54 (2006) 1035–1040.
[28] V.Y. Gertsman, K. Tangri, Modelling of intergranular damage propagation, Acta Mater. 45 (1997) 4107–4116.
[29] V.K.S. Shante, S. Kirkpatrick, An introduction to percolation theory, Adv. Phys. 20 (1971) 325–357.
[30] C.A. Schuh, R.W. Minich, M. Kumar, Connectivity and percolation in simulated grain-boundary networks, Philos. Mag. 83 (2003) 711–726.
[31] E.G. Doni, G.L. Bleris, Study of special triple junctions and faceted boundaries by means of the CSL model, Phys. Status Solidi A 110 (1988) 383–395.
[32] K. Miyazawa, Y. Iwasaki, K. Ito, Y. Ishida, Combination rule of Σ values at triple

junctions in cubic polycrystals, Acta Crystallogr. A 52 (1996) 787–796.
[33] V.Y. Gertsman, Geometrical theory of triple junctions of CSL boundaries, Acta Crystallogr. A 57 (2001) 369–377.
[34] V.Y. Gertsman, C.H. Henager, Grain boundary junctions in microstructure generated by multiple twinning, Interface Sci. 11 (2003) 403–415.
[35] V.Y. Gertsman, Coincidence Site Lattice Theory of Triple Junctions and Quadruple Points. Science and Technology of Interfaces, John Wiley & Sons, Inc, 2002, pp. 387–398.
[36] F.J. Humphreys, Review Grain and subgrain characterisation by electron backscatter diffraction, J. Mater. Sci. 36 (2001) 3833–3854.
[37] C. Cayron, Quantification of multiple twinning in face centred cubic materials, Acta Mater. 59 (2011) 252–262.
[38] H.C.H. Carpenter, S. Tamura, The formation of twinned metallic crystals, Proc. R. Soc. Lond. 113 (1926) 161–182.
[39] W.G. Burgers, J.C. Meijs, T.J. Tiedema, Frequency of annealing twins in copper crystals grown by recrystallization, Acta Metall. 1 (1953) 75–78.
[40] S. Dash, N. Brown, An investigation of the origin and growth of annealing twins, Acta Metall. 11 (1963) 1067–1075.
[41] H. Gleiter, The formation of annealing twins, Acta Metall. 17 (1969) 1421–1428.
[42] S. Mahajan, C.S. Pande, M.A. Imam, B.B. Rath, Formation of annealing twins in f.c.c. crystals, Acta Mater. 45 (1997) 2633–2638.
[43] W. Wang, S. Lartigue-Korinek, F. Brisset, A.L. Helbert, J. Bourgon, T. Baudin, Formation of annealing twins during primary recrystallization of two low stacking fault energy Ni-based alloys, J. Mater. Sci. 50 (2015) 2167–2177.
[44] M.A. Meyers, L.E. Murr, A model for the formation of annealing twins in F.C.C. metals and alloys, Acta Metall. 26 (1978) 951–962.
[45] B.W. Reed, M. Kumar, Mathematical methods for analyzing highly-twinned grain boundary networks, Scr. Mater. 54 (2006) 1029–1033.
[46] G. Gottstein, Annealing texture development by multiple twinning in f.c.c. crystals, Acta Metall. 32 (1984) 1117–1138.
[47] C. Cayron, Multiple twinning in cubic crystals: geometric/algebraic study and its application for the identification of the Σ3n grain boundaries, Acta Crystallogr. A 63 (2007) 11–29.
[48] C.V. Kopezky, A.V. Andreeva, G.D. Sukhomlin, Multiple twinning and specific properties of Σ = 3n boundaries in f.c.c. crystals, Acta Metall. Mater. 39 (1991) 1603–1615.
[49] T. Liu, S. Xia, B. Wang, Q. Bai, B. Zhou, C. Su, Grain orientation statistics of grain-clusters and the propensity of multiple-twinning during grain boundary engineering, Mater. Des. 112 (2016) 442–448.
[50] P. Haasen, How are new orientations generated during primary recrystallization? Metall. Trans. A. 24 (1993) 1001–1015.
[51] F. Hanning, D.L. Engelberg, Metallographic screening of grain boundary engineered type 304 austenitic stainless steel, Mater. Charact. 94 (2014) 111–115.
[52] A.C. Lewis, J.F. Bingert, D.J. Rowenhorst, A. Gupta, A.B. Geltmacher, G. Spanos, Two- and three-dimensional microstructural characterization of a super-austenitic stainless steel, Mater. Sci. Eng. A 418 (2006) 11–18.
[53] F.X. Lin, A. Godfrey, D.J. Jensen, G. Winther, 3D EBSD characterization of deformation structures in commercial purity aluminum, Mater. Charact. 61 (2010) 1203–1210.
[54] D.J. Rowenhorst, A.C. Lewis, G. Spanos, Three-dimensional analysis of grain topology and interface curvature in a beta-titanium alloy, Acta Mater. 58 (2010) 5511–5519.
[55] C. Zhang, A. Suzuki, T. Ishimaru, M. Enomoto, Characterization of three-dimensional grain structure in polycrystalline iron by serial sectioning, Metall. Mater. Trans. A 35a (2004) 1927–1933.
[56] M. Groeber, M. Jackson, DREAM.3D: a digital representation environment for the analysis of microstructure in 3D, Integr. Mater. Manuf. Innov. 3 (2014) 1–17.
[57] U. Ayachit, The ParaView Guide: A Parallel Visualization Application, Kitware, 2015.
[58] M. Groeber, S. Ghosh, M. Uchic, D. Dimiduk, A framework for automated analysis and simulation of 3D polycrystalline microstructures. Part 2: synthetic structure generation, Acta Mater. 56 (2008) 1257–1273.
[59] Y. Bhandari, S. Sarkar, M. Groeber, M.D. Uchic, D.M. Dimiduk, S. Ghosh, 3D polycrystalline microstructure reconstruction from FIB generated serial sections for FE analysis, Comput. Mater. Sci. 41 (2007) 222–235.
[60] D.G. Brandon, The structure of high-angle grain boundaries, Acta Metall. 14 (1966) 1479–1484.
[61] V.Y. Gertsman, M. Janecek, K. Tangri, Grain boundary networks in AISI 316L stainless steel, Phys. Status Solidi A 157 (1996) 241–247.
[62] A. Telang, A.S. Gill, M. Kumar, S. Teysseyre, D. Qian, S.R. Mannava, V.K. Vasudevan, Iterative thermomechanical processing of alloy 600 for improved resistance to corrosion and stress corrosion cracking, Acta Mater. 113 (2016) 180–193.
[63] G. Gottstein, L.S. Shvindlerman, Grain boundary junction engineering, Scr. Mater. 54 (2006) 1065–1070.
[64] A. Ullah, G.Q. Liu, J.H. Luan, W.W. Li, M.U. Rahman, M. Ali, Three-dimensional visualization and quantitative characterization of grains in polycrystalline iron, Mater. Charact. 91 (2014) 65–75.
[65] V. Gertsman, Coincidence site lattice theory of multicrystalline ensembles, Acta Crystallogr. A 57 (2001) 649–655.
[66] S.F. Li, J.K. Mason, J. Lind, M. Kumar, Quadruple nodes and grain boundary connectivity in three dimensions, Acta Mater. 64 (2014) 220–230.
[67] B.W. Reed, R.W. Minich, R.E. Rudd, M. Kumar, The structure of the cubic coincident site lattice rotation group, Acta Crystallogr. A 60 (2004) 263–277.
[68] V.Y. Gertsman, S.M. Bruemmer, Study of grain boundary character along intergranular stress corrosion crack paths in austenitic alloys, Acta Mater. 49 (2001) 1589–1598.